Supplementary materials

Mounting the animal

Pupae were mounted on a custom platform made of adhesive putty (Scotch adhesive putty, 3M, Minnesota, USA) on the ventral side of the thorax (figure S1). In the respiratory trials at Virginia Tech, no other adhesive was used. In X-ray trials at Argonne National Laboratory, we additionally used a small droplet of nail polish (Revlon, NY, USA) to ensure that the specimen would not be disturbed when the translation stage was moved. Despite the adhesion, in this position the pupa was able to move the abdomen freely.

Figure S1: Pupa mounted on a custom made platform. Scale bar is 3mm.

Measuring abdominal movements

Abdominal movements were recorded with either a video camera or an infrared (IR) sensor. IR sensors emit light in the infrared spectrum that is read by a detector, which is sensitive to those wavelengths. When an object is within range of the emitter, the light bounces off the object and the detector reports the intensity of the light. The intensity of the returning light depends on the proximity of the object, as well as its geometry and surface properties. Therefore, the IR signal does not report the true displacement of the

abdomen. In our experiments, the IR sensor (SUNX FD-T80, Panasonic, Iowa, USA) was positioned 2-3 cm from the animal, aimed at its posterior side facing the abdomen. The cyclic abdominal movements changed the intensity of the returning light, appearing as a pulse in the output signal. In some trials, we used a video camera (NEX-VG10, SONY, California, USA) positioned on the lateral side of the animal to determine the details of abdominal movements with greater precision. The recorded images were analyzed frame-by-frame using a custom MATLAB code (available upon request). The recorded images show that the abdomen compresses dorsoventrally and the entire abdomen swings rhythmically back and forth toward the ventral direction (figure S2). The maximum displacement occurs in the cerci at the end of the abdomen; therefore, we measured the displacement here. To process the footage, we cropped the images to include only the cerci and subtracted the background from each frame. This rendered the cerci easily visible so that they could be automatically tracked using a point detection algorithm (figure S2).

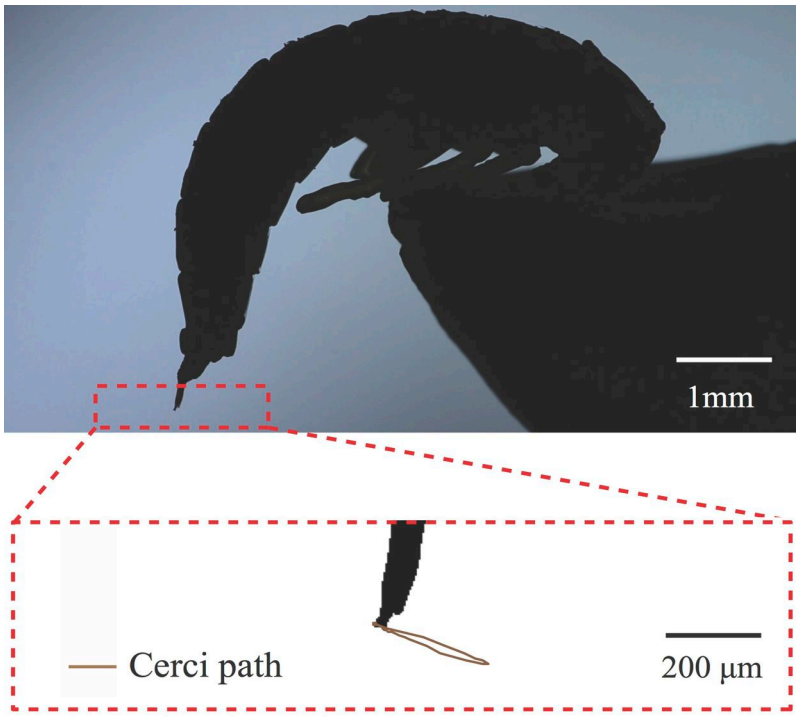

Figure S2: Method for measuring displacement during abdominal pumping, using the tip of the cerci. The image is a video frame recorded from the lateral view video camera.

CO_2 measurement and analysis

A custom-made respirometry chamber (28 mL, 25×25×45 mm^3) was used to record the CO_2 emission of the pupae (figure S3 and S4). The chamber included a small port at the top for inserting a pressure transducer into the dorsal side of the pupa. The hole to the chamber was sealed with adhesive putty. The pressure signal was recorded in real time, but the CO_2 data were not instantaneous, a characteristic of flow-through respirometry systems [1, 2]. The instantaneous CO_2 signal was recovered using the methods described by Pendar [3]. The aim of this setup was to compare the patterns of the abdominal movement and hemolymph pressure during CO_2 burst periods versus interburst periods. Therefore, the relevant instantaneous respiratory information was simply the times of the start and end of the CO_2 burst. We used the following method to find the burst and interburst durations from the recorded data.

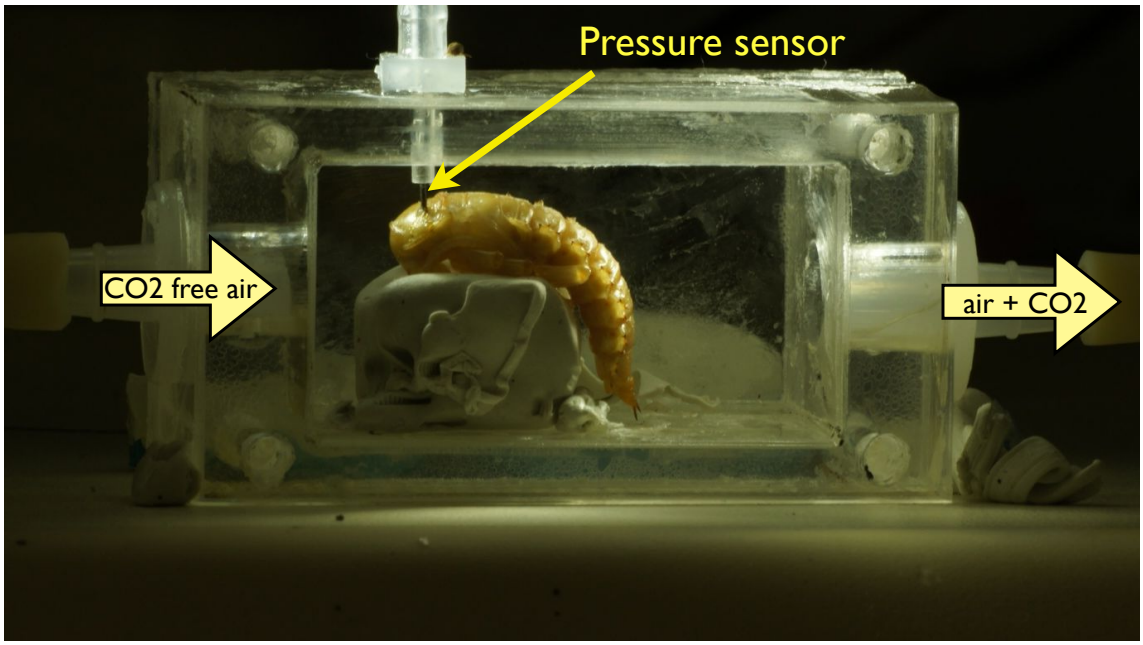

Figure S3: A pupa mounted inside the respirometry chamber, with the pressure sensor inserted in the prothorax. In these trials, abdominal movement was recorded with a video camera (not shown).

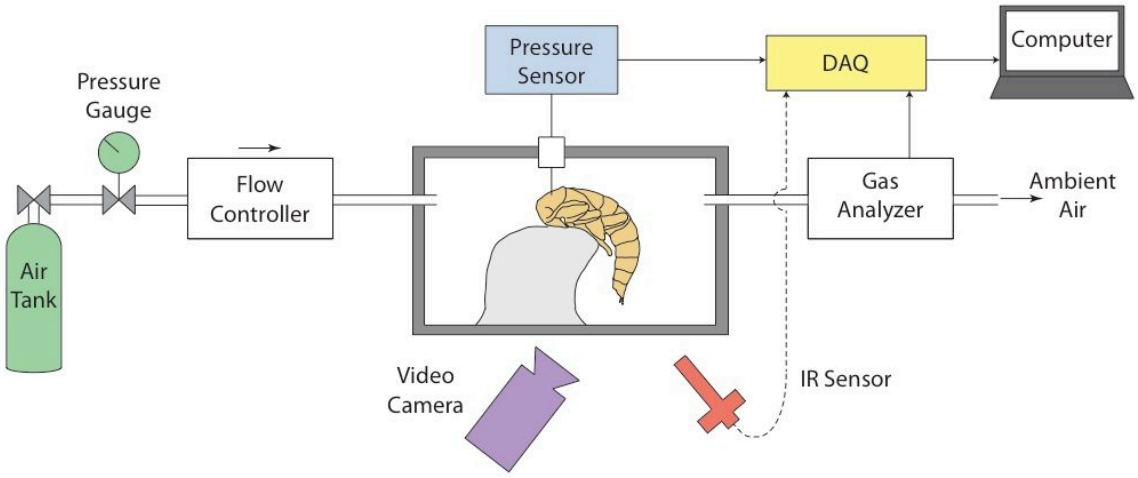

Figure S4: Schematic of the setup for measurement of CO_2, pressure, and abdominal movement. For abdominal movement recordings, either the IR sensor or video camera was used. The actual placement of the video camera was such that it was orthogonal to the pupa, in lateral view (see figure S2). The IR sensor was placed 2~3 cm from the abdomen from the posterior side.

Washout correction: Due to washout, if a pulse of CO_2 of very short duration is injected into the chamber, it does not appear as a short duration pulse in the output (the recorded signal) [1, 2, 4]. After a delay, the signal gradually rises and then exponentially decays. The shape of the output signal (also known as the impulse response) depends on many variables, including the flow rate and volume of the chamber. For any short input signal, the output signal has a lag at the beginning (τ_d) and exhibits an elongated duration (τ_l) (figure S5a). To determine these constants, we injected a short (200 ms) pulse of CO_2 into the chamber at the location where the animal would be. The lag time and duration of the signal were then determined by comparing the output signal with a threshold horizontal value. We arbitrarily considered 2% of the maximum of the output as the threshold.

Finding the start and end of CO_2 bursts: The start of a burst was defined to occur when the output crossed above the threshold value, and the end was defined as the last time it crosses and stayed below the threshold. Once the burst was identified, the following algorithm was used to find the burst duration (figure S5):

1- Find the start and end of the output signal (using 2% threshold criteria; figure S5b).

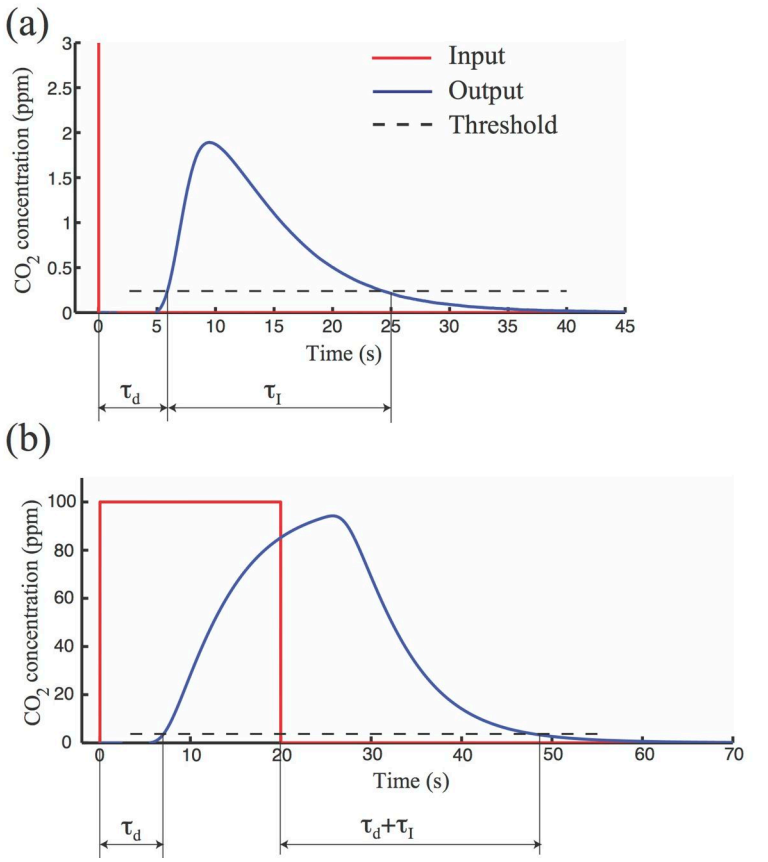

Figure S5: Method to recover the burst periods from the recorded CO_2 data. (a) τ_d and τ_I were determined from the impulse response of the system using a short injection of CO_2 (red). The output (blue) is the recorded CO_2 data. (b) To test this method, we took a simulated input of long duration (red) and convolved it with the impulse response to simulate the output signal (blue). Then we applied the correction method to the output to recover the duration of the input, and compared the recovered value to the original input.

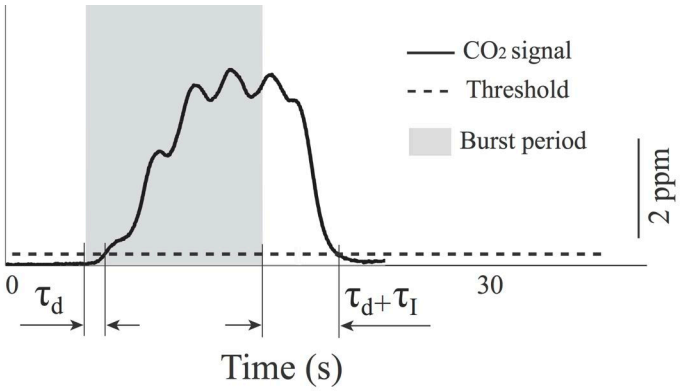

Figure S6: An example of an experimentally-recorded CO_2 burst and post-hoc temporal correction, taken from the pupa reported in figure 2a. The inlet flow rate was 2.5 L/min.

2- Shift the start and end points (from step 1) to the left by τ_d and $\tau_d + \tau_I$, respectively (figure S5b).

This method was tested in a simulation with a custom MATLAB code. This code simulates an insect's respirometry pattern and determines the respirometry output for any given CO_2 burst. To find the output, it simply convolves the given input with the impulse response of the system, which was determined experimentally. After finding the output signal, it uses the described algorithm to find the start and end of the given CO_2 burst. We tested the method for a flow rate of 2.5 L/min (the same as in animal trials) and input pulses with durations of 1, 2, 3, 5, 10, and 20 seconds. The average error for the start and end points were 0.19±.02 and 0.192±.07 s, respectively. The method was tested for rectangular inputs; however, in pupae, the shape of the burst is not known. Therefore, the true error may be larger. This method was applied to the recorded CO_2 signal of pupae to find the burst periods (figure S6).

Pressure signals

The pressure sensors produce an analog light signal read through a signal conditioner (Samba 202, Samba Sensors, Gothenburg, Sweden). This voltage signal is converted to pressure using an experimentally determined transform equation. We then used a custom MATLAB code to identify the pressure pulses and to determine their magnitude and duration. We only considered pulses with magnitudes and durations greater than 200 Pa and 0.2 s, respectively. We calculated the peak of each pulse as the local maximum of the signal. To find the baseline between two pulses, we took the average of the lowest 5% of data points between pulse peaks. The start of each pulse was defined as the time at which the value rises above the calculated baseline before rising to the peak value. The end of each pulse was defined as the time when the signal fell below the baseline after this peak.

Calibration of the sensors: An adjustable water column in a long graded tube was used to calibrate the transducers. The sensors were inserted in the tube and then filled with water. The level of the water was adjusted with a valve at the bottom of the tube. The output voltage of the sensor was recorded at 12 heights and the gage pressure was determined from the corresponding water heights ($P = \rho g h$, where P = pressure, ρ = density of

water, h = height of water column). The calibration parameters were determined by using a least-squares regression fit to all the data points.

Filtering the noise and drift: In general, pressure sensors suffer from two types of errors: random error, manifest as noise, and bias error, manifest as drift. To characterize both sources of error, we conducted a long-term recording of hydrostatic pressure by immersing the pressure sensor in a fixed position in a water bath for 35 hours, using a sampling frequency of 100 Hz (figure S7a). The noise was consistent throughout the trial, with a magnitude of ~12 Pa, calculated as one standard deviation of the mean (figure S7b,c). To filter this noise, we applied a simple moving average to our data (figure S7d). To determine the window size of the filter, we applied three arbitrary window sizes and chose the minimum value (n=11) that significantly reduced the noise, while still retaining the essential features of the beetle's observed pressure pulses (figure S7e). After applying this filter, the magnitude of the noise was ~4 Pa (=1 S.D.).

In the water bath trial, we observed a drift of ~150 Pa over the course of 35 hours, with a maximum rate of change of ~1 Pa/s. The magnitude of this change is much smaller than the observed pressure pulses in the beetles, which were on the order of ~10,000 Pa/s. To remove drift from our data, we assumed that the beetle exhibited a resting baseline pressure, and pressure pulses occurred on top of this baseline. Because we were only interested in the magnitude of the pressure pulses, and because the absolute baseline pressure could not be determined, we assumed that the baseline pressure in the hemolymph was zero. In practice, we corrected for drift in our data in consecutive 5-minute blocks. For each block of data, we defined the baseline as the average of the lowest 5% of the pressure values within that block (figure S7f). We then subtracted this value from all of the data points in that block (figure S7g).

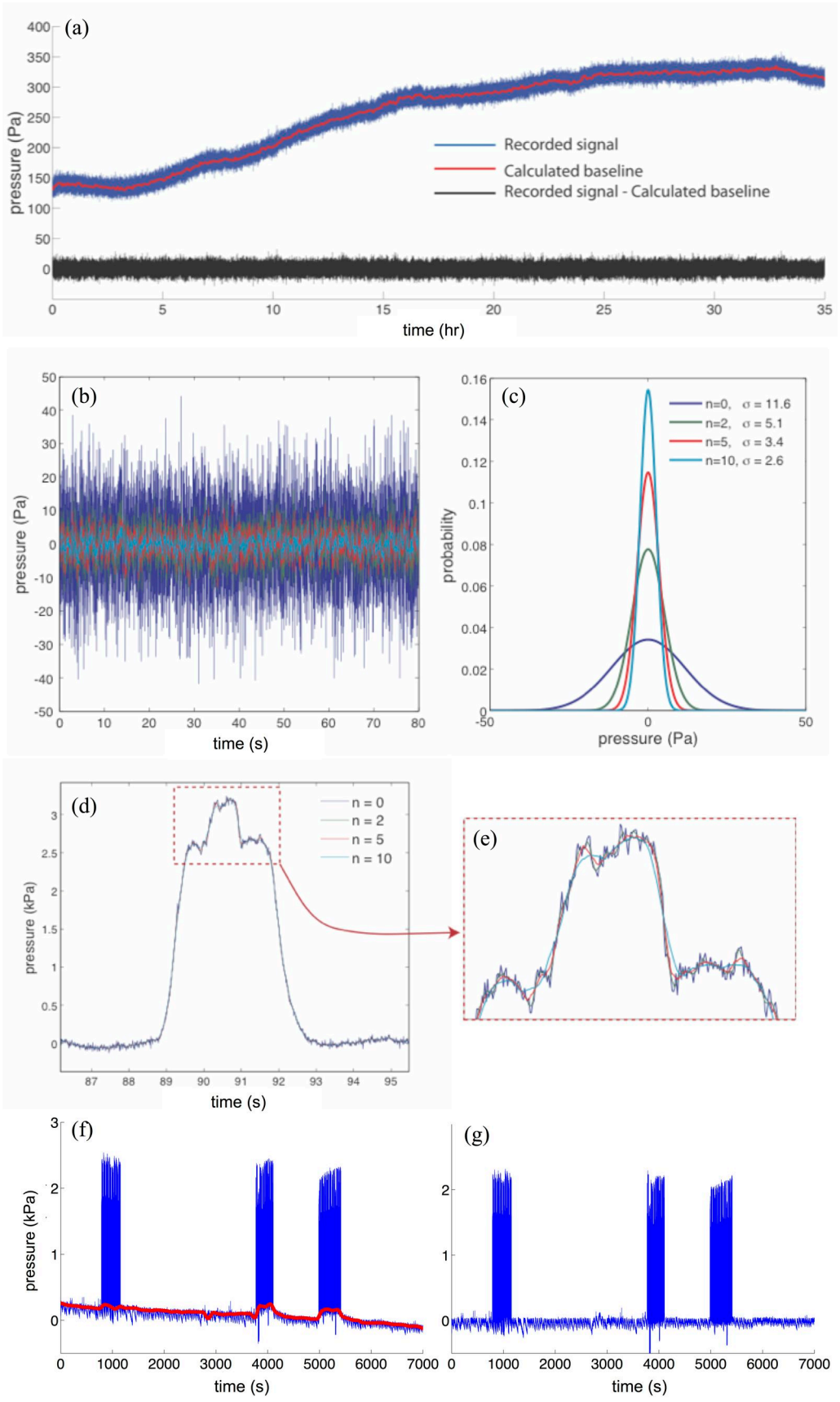
(a)
pressure (Pa)
time (hr)
Recorded signal
Calculated baseline
Recorded signal - Calculated baseline
(b)
pressure (Pa)
time (s)
(c)
probability
pressure (Pa)
n=0, σ = 11.6
n=2, σ = 5.1
n=5, σ = 3.4
n=10, σ = 2.6
(d)
pressure (kPa)
time (s)
n = 0
n = 2
n = 5
n = 10
(e)
(f)
pressure (kPa)
time (s)
(g)
time (s)

142

Figure S7: Noise and drift analysis of the pressure sensor. (a) Static pressure recording from a water bath, with the sensor immersed at one depth and held in place. This trace shows a slow change in the pressure over time, a drift of ~150 Pa. Subtracting the baseline pressure from the signal eliminates the slow drift. (b) Representative details of the pressure trace from (a), showing the effect of different moving average window sizes on the data. As shown in the legend in (c), a moving average was applied to the data using window sizes of 5 (n=2), 11 (n=5), and 21 (n=10). The data here were first baseline corrected, and so their average is zero. (c) Histogram of the original data and filtered data shows the effect of the moving average on the distribution of noise. The standard deviation of the noise decreases with increasing window size of the filter. (d, e) The effect of the moving average on a representative pressure pulse recorded in the pupa's hemolymph. These plots show that a stronger filter decreases the temporal resolution of the signal. We chose to use a window size of 11 points (n=5) because it decreases the noise without considerably changing the shape of the pulse. (f, g) Effect of baseline correction on a representative pressure trace from the hemolymph of a pupa. The calculated baseline is shown in red overlaying the original data in (f), and the corrected data are shown in (g).

Statistical analysis

All the statistical comparisons were conducted using a Wilcoxon rank sum test, with significance determined at the 5% level, using MATLAB.

Prediction of tube collapse from pressure data

In X-ray trials, the behavior of tracheal tubes during each pressure pulse was determined from the recorded videos (figure 1, Table S1). To predict tube collapse from the pressure signal, we clustered the pressure pulses of each trial separately into two groups, using the k-means clustering method [5]. This method clusters the data into k groups using initial means and iterative calculations of the centroid of each group [5]. In practice, we employed the method using the 'kmeans' function in MATLAB. We hypothesized that the group with lower average pressure would be associated with tube collapse events (figure 1, table S1) and then compared the predictions with tube collapse events in the X-ray movies. The accuracy of the prediction was 95.73%.

Table S1: X-ray trial analysis. The distribution of the pressure points can be used to predict the presence or absence of tube collapse (see figure 1-e).

		tube collapse		no tube collapse		
	X-ray movie number	number of pressure pulses	average pressure (kPa)	number of pressure pulses	average pressure (kPa)	Accuracy of prediction (%)
Pupa 1	1	12	1.56±0.11	19	2.01±0.05	96.77
	2	12	1.53±0.13	16	2.03±0.10	96.3
	3	7	1.58±0.08	7	2.05±0.07	100
	4	12	1.63±0.10	25	2.13±0.07	97.30
	5	4	1.61±0.06	5	1.97±0.08	100
	6	16	1.67±0.12	45	2.17±0.05	98.36
	7	15	1.67±0.12	19	2.14±0.06	97.06
Pupa 2	8	34	1.67±0.13	43	2.20±0.16	96.10
	9	9	1.79±0.14	18	2.23±0.10	96.30
	10	7	1.73±0.07	10	1.94±0.09	88.4
	11	3	1.44±0.02	4	1.76±0.09	100
Pupa 3	12	12	1.23±0.10	34	1.58±0.08	95.65
	13	9	1.31±0.10	2	1.70±0.05	90.91
	14	8	1.51±0.21	29	1.71±0.09	83.78
Pupa 4	15	6	1.03±0.04	6	1.30±0.06	100
	16	7	0.94±0.07	8	1.20±0.05	100
	17	11	0.98±0.03	6	1.24±0.03	100
	18	9	1.100.10	11	1.32±0.07	90
	19	11	1.01±0.05	22	1.25±0.04	100
	20	14	1.00±0.05	15	1.23±0.03	96.55

Table S2: Summary data of abdominal movement, hemolymph pressure, and CO_2 emission from video-recorded trials.

		burst period			interburst period			accuracy of prediction based on	
	sequence number	number of pulses	pressure (kPa)	abdomen movement (μm)	number of pulses	pressure (kPa)	abdomen movement (μm)	pressure (%)	Abdominal movement (%)
Pupa 5	1	54	1.38±0.04	47.28±2.38	182	1.56±0.04	38.51±3.60	97.46	94.49
	2	13	1.21±0.02	48.89±1.16	28	1.37±0.03	40.61±2.78	100	92.68
Pupa 6	1	50	1.47±0.06	64.37±3.11	130	1.82±0.12	43.53±6.54	92.78	93.89
	2	18	1.51±0.09	52.10±6.56	147	1.80±0.04	30.09±2.12	97.58	99.39
Pupa 7	1	104	1.71±0.09	81.04±4.74	292	1.88±0.15	68.71±5.58	80.30	90.90
	2	22	1.85±0.11	80.96±9.51	45	1.98±0.08	67.93±4.92	73.13	80.60

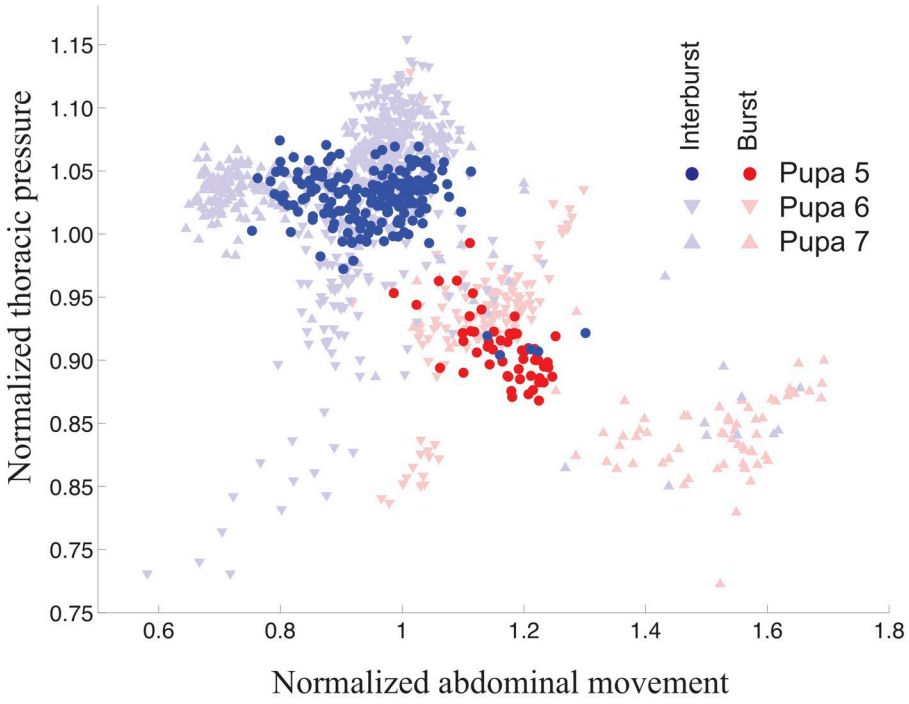

Figure S8: Summary plot of abdominal movement vs. maximum pressure for each abdominal pump/pressure pulse for three pupae. Events during burst or interburst periods are indicated by color (red and blue, respectively). Pressure and abdominal displacement values were normalized by the total average across all three pupae.

Table S3: Summary data of hemolymph pressure and CO_2 emission from IR-recorded trials.

		burst period		interburst period		
	sequence number	number of pulses	pressure (kPa)	number of pulses	pressure (kPa)	Accuracy of prediction (%)
Pupa 8	1	54	1.63±0.24	116	2.17±0.07	94.70
	2	43	1.50±0.19	80	2.10±0.05	95.93
	3	53	1.48±0.22	152	2.00±0.14	93.66
	4	53	1.38±0.06	268	1.93±0.17	92.52
	5	31	1.42±0.16	206	1.93±0.16	93.25
Pupa 9	1	53	1.65±0.19	122	2.23±0.07	96
	2	53	1.57±0.17	111	2.04±0.33	91.46
	3	59	1.54±0.16	117	2.03±0.15	92.05
	4	140	0.90±0.07	263	1.09±0.11	76.92
Pupa 10	1	32	0.59±0.16	122	1.04±0.09	95.45
Pupa 11	1	67	1.55±0.26	340	1.95±0.13	92.63
	2	25	1.41±0.22	330	1.87±0.13	90.99
Pupa 12	1	8	1.97±0.08	106	2.13±0.05	92.11
Pupa 13	1	96	1.63±0.06	344	1.84±0.09	88.18
	2	88	1.75±0.05	405	1.95±0.09	79.92
Pupa 14	1	9	1.56±0.08	46	1.77±0.09	90.91

Prediction of CO_2 emission from pressure data

Abdominal pumping, hemolymph pressure, and CO_2 emission were recorded simultaneously in 10 pupae. For the first 7 pupae, abdominal pumping was recorded with IR, and in 3 additional trials, a video camera was used to more precisely determine the magnitude of the abdominal movement. We clustered pressure pulses (all pupae) and abdominal movements (3 pupae) to predict the CO_2 emission pattern (open/closed phases) and then compared the prediction with the real CO_2 signal (figure 2 in the paper, figure S8, and tables S2 and S3). The average accuracy of the prediction based on abdominal movement and pressure pulses was 92.7% and 88.9% respectively.

References

1. Lighton, J.R. 2012 'Instantaneous' metabolic measurement *J Exp Biol* **215**, 1605-1606.

2. Lighton, J. & Halsey, L. 2011 Flow-through respirometry applied to chamber systems: pros and cons, hints and tips. *Comp. Biochem. Physiol., A: Comp. Physio.* **158**, 265-275.

3. Pendar, H. 2014 The mechanical linkage of abdominal movements and the respiratory system in beetles [PhD Dissertation], Virginia Tech.

4. Pendar, H. & Socha, J. 2014 Computational methods to determine the instantaneous respiratory patterns of animals from respirometry data. In *Integr Comp Biol* (pp. E162-E162), Oxford Univ Press Inc Journals Dept, 2001 Evans Rd, Cary, NC 27513 USA.

5. MacQueen, J. 1967 Some methods for classification and analysis of multivariate observations. In *Proc. Fifth Berkeley Symp. on Math. Statist. and Prob* (pp. 281-297), California, USA.

Data supplement

The following plots document the original data from each pupa from the CO_2 trials, all of which include pressure measurements, and some of which include abdominal movement measurements. Numerical data and video data are permanently available online on Dryad (doi:10.5061/dryad.90sj5).

Pupa 5 - sequence 1

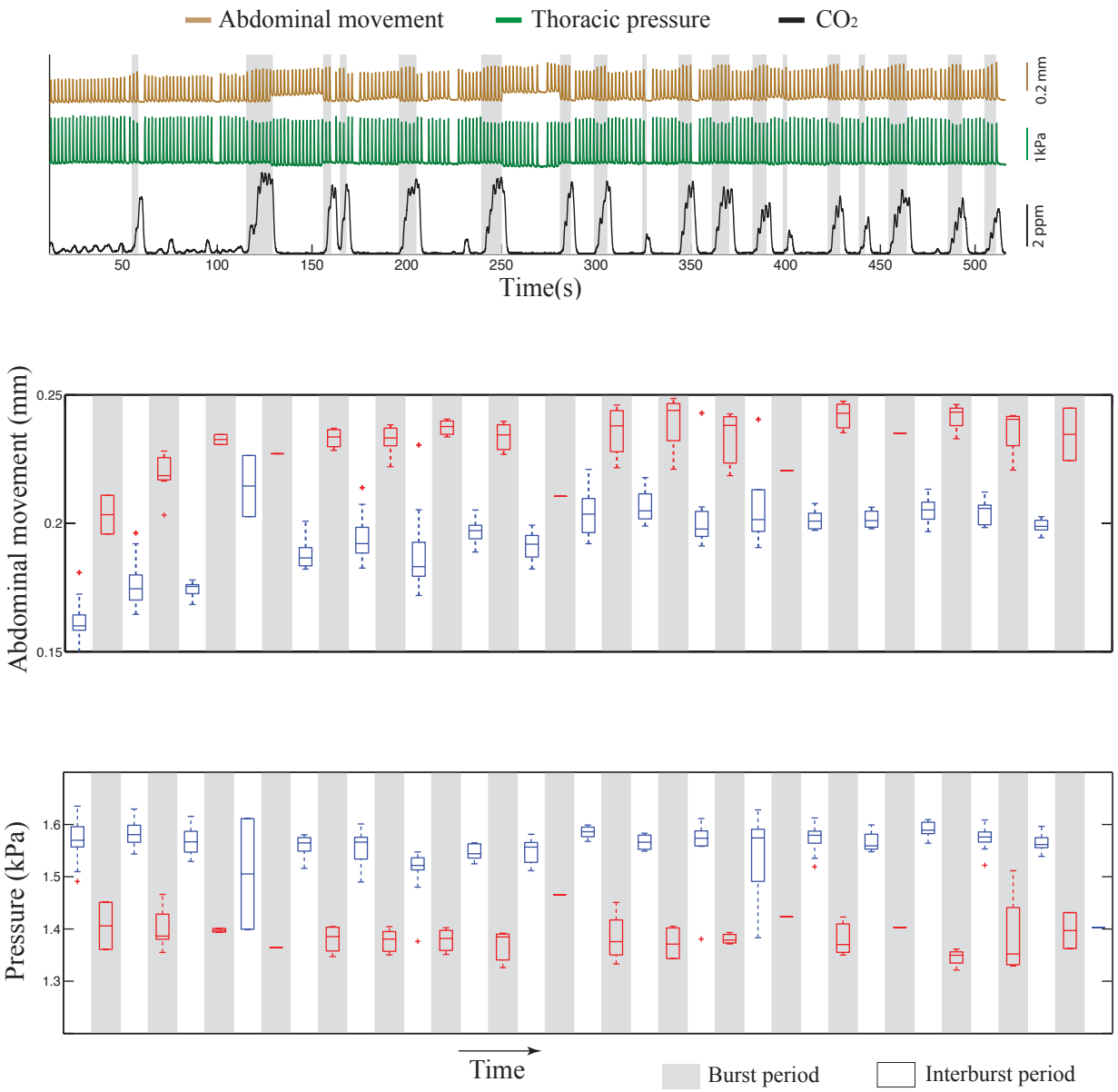

Pupa 5 - sequence 2

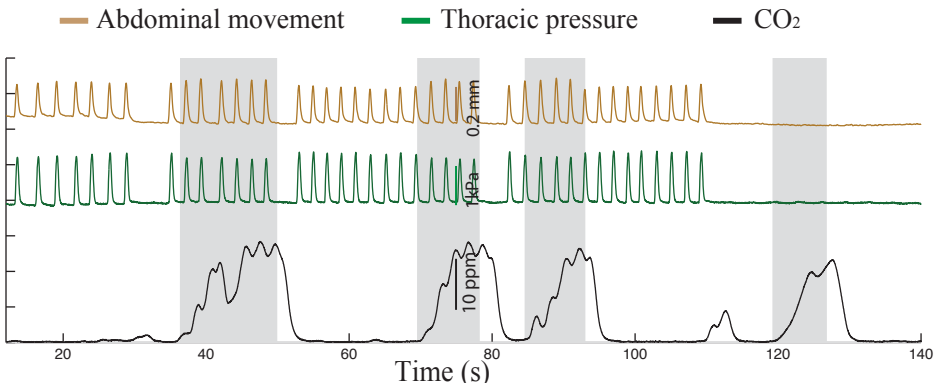

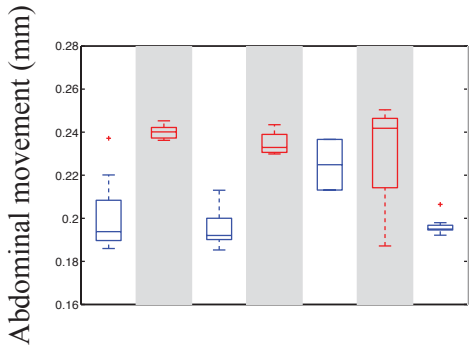

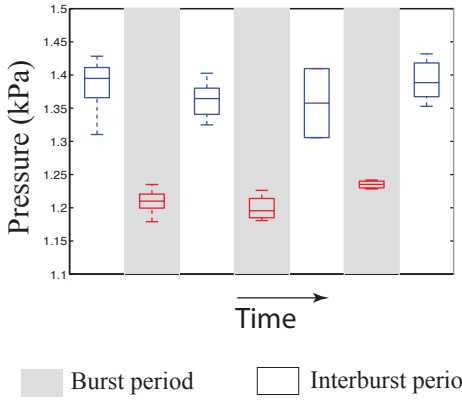

Pupa 6 - sequence 1

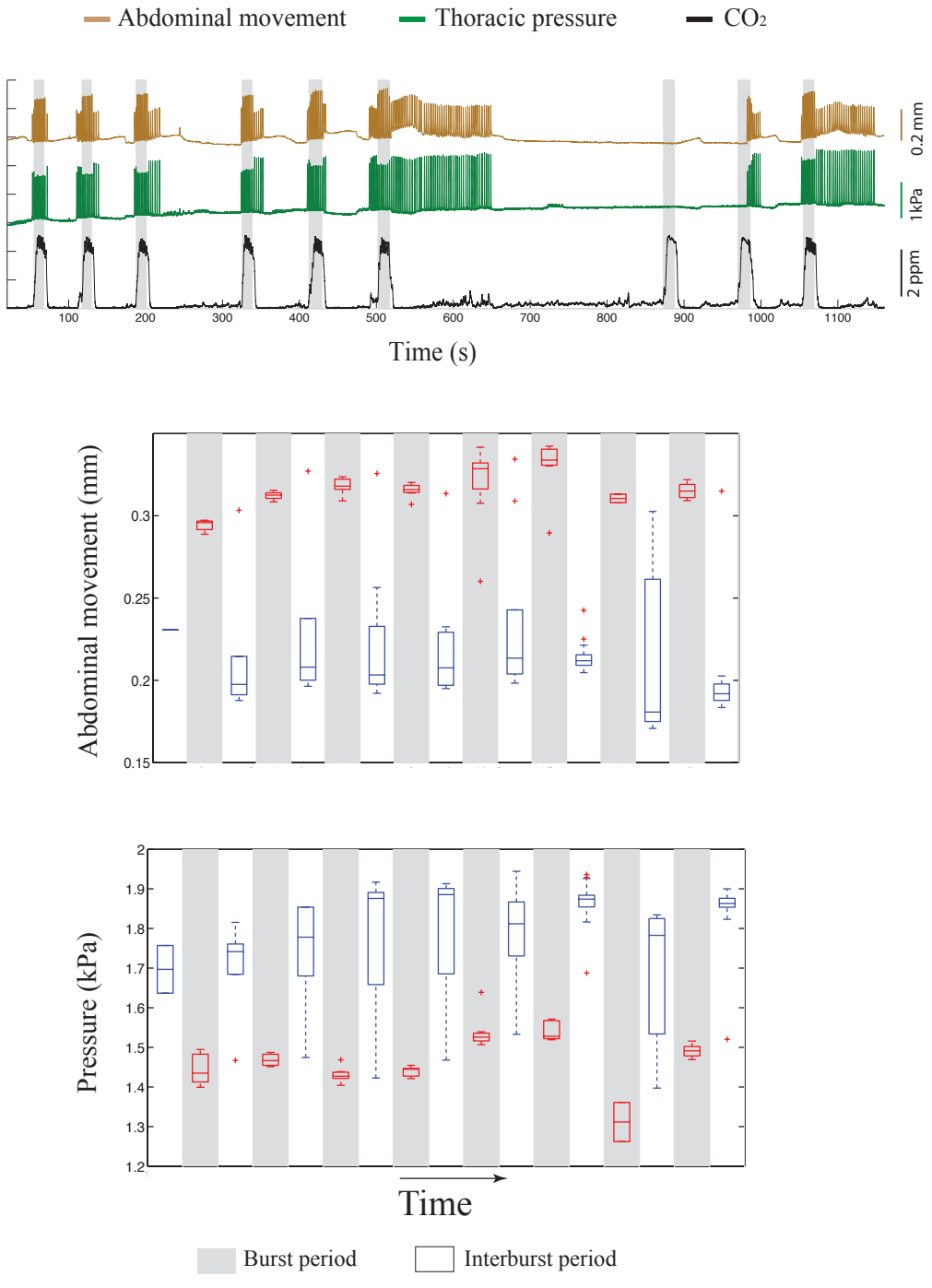

Pupa 6 - sequence 2

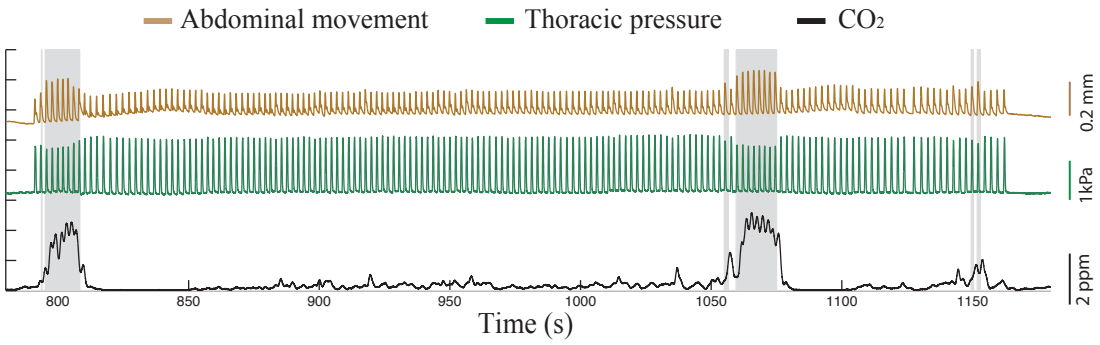

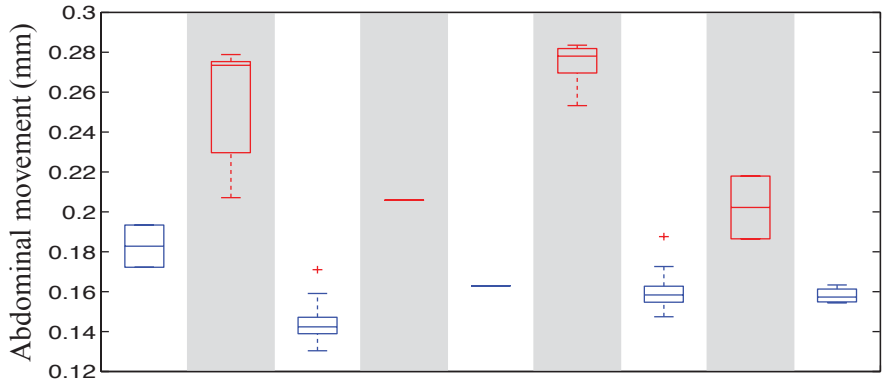

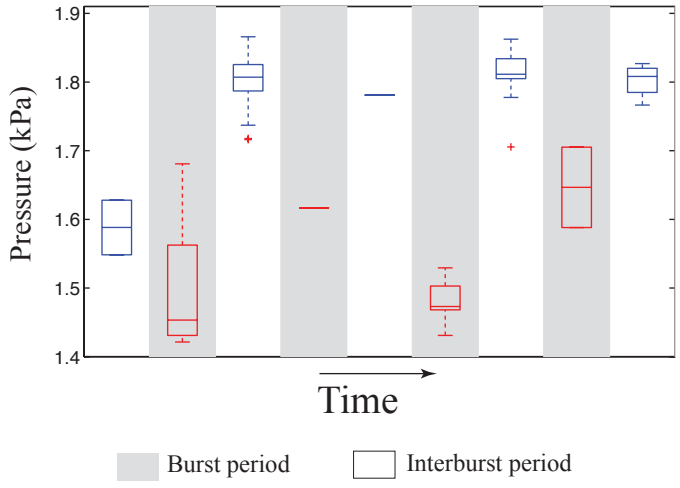

Pupa 7 - sequence 1

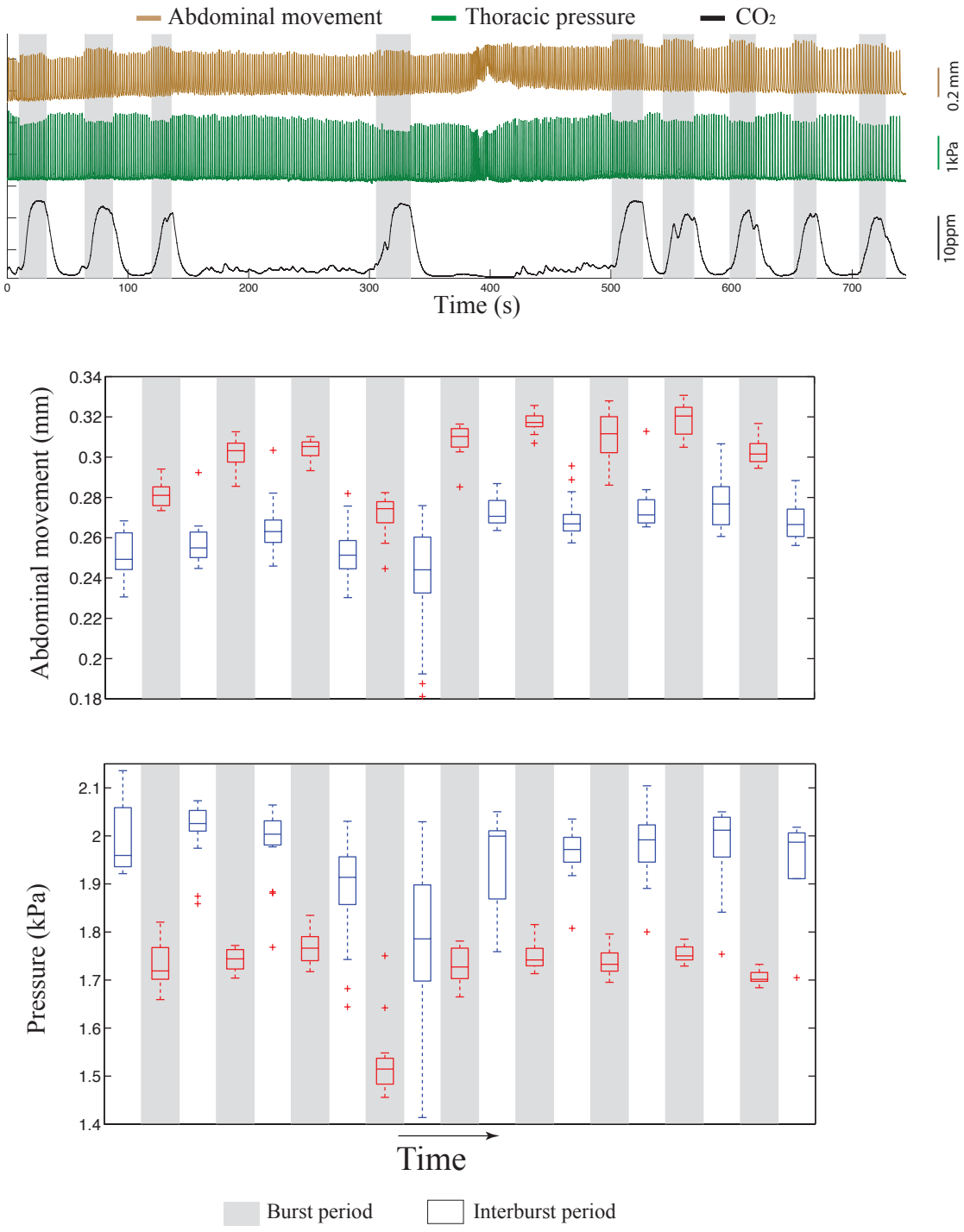

Pupa 7 - sequence 2

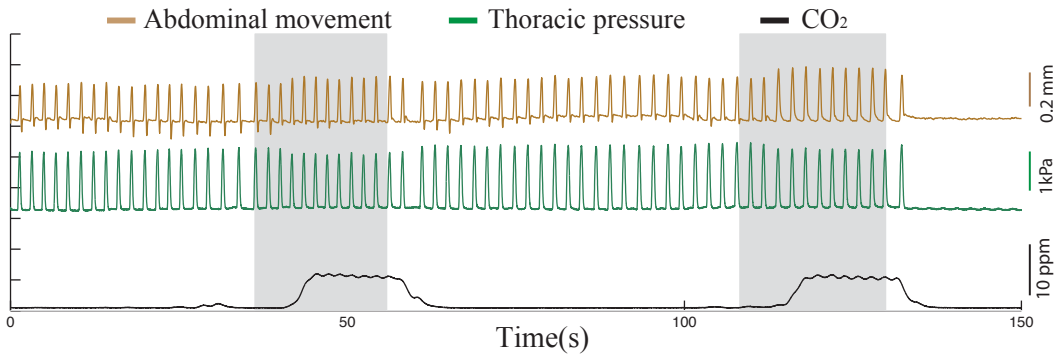

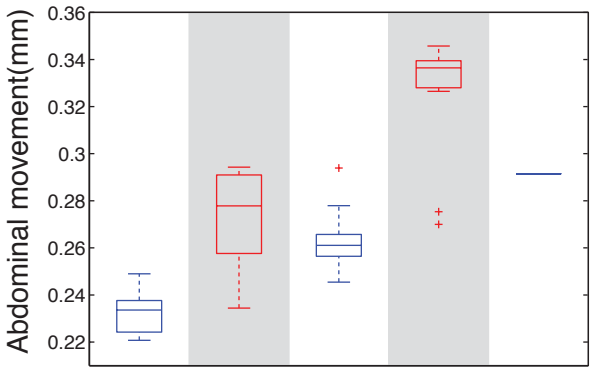

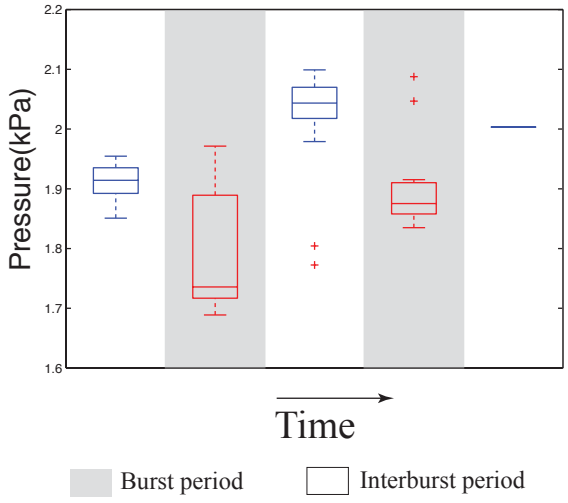

Pupa 8 - sequence 1

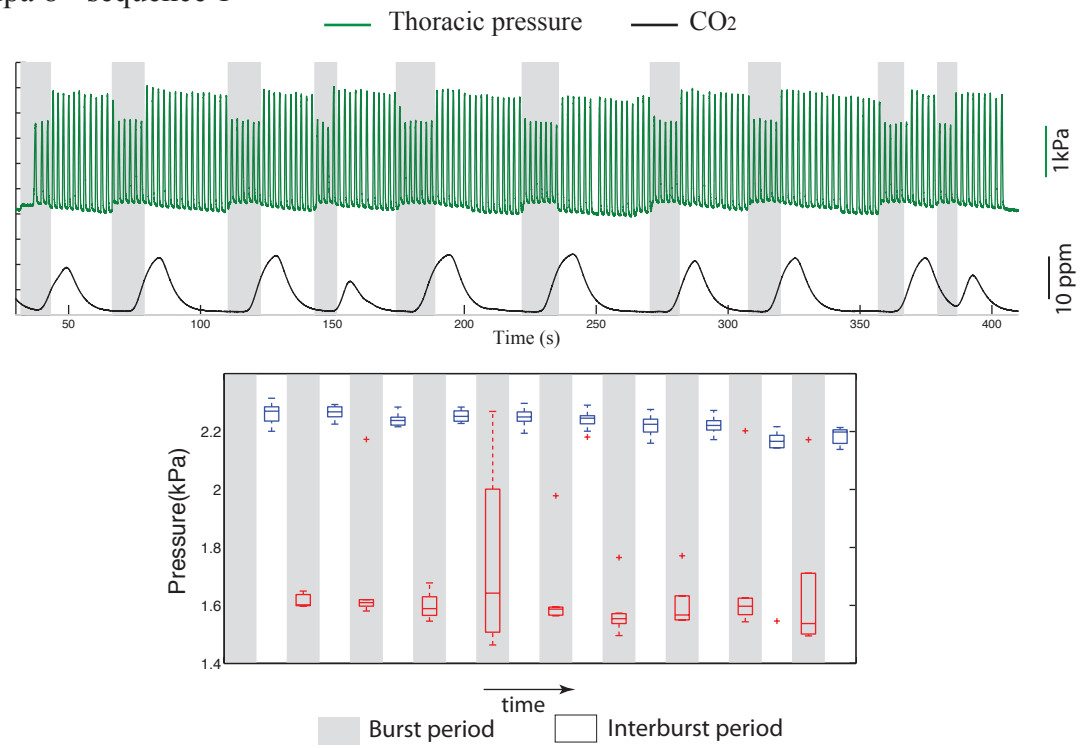

Pupa 8 - sequence 2

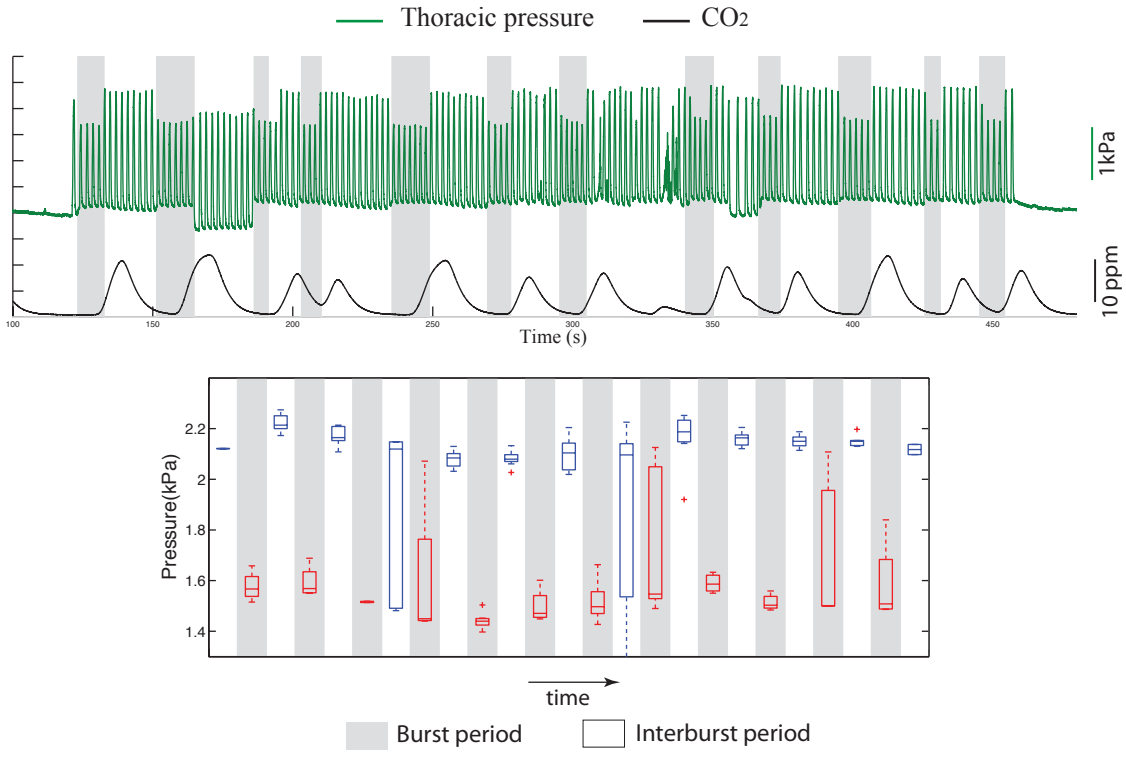

Pupa 8 - sequence 3

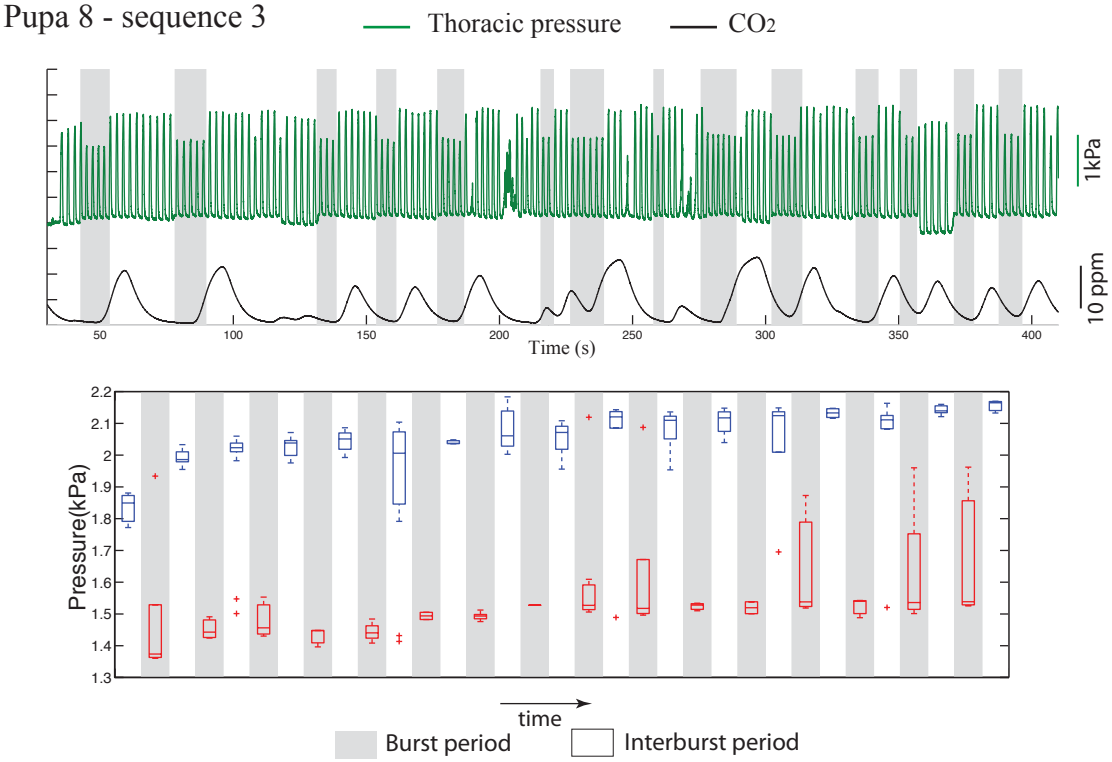

Pupa 8 - sequence 4

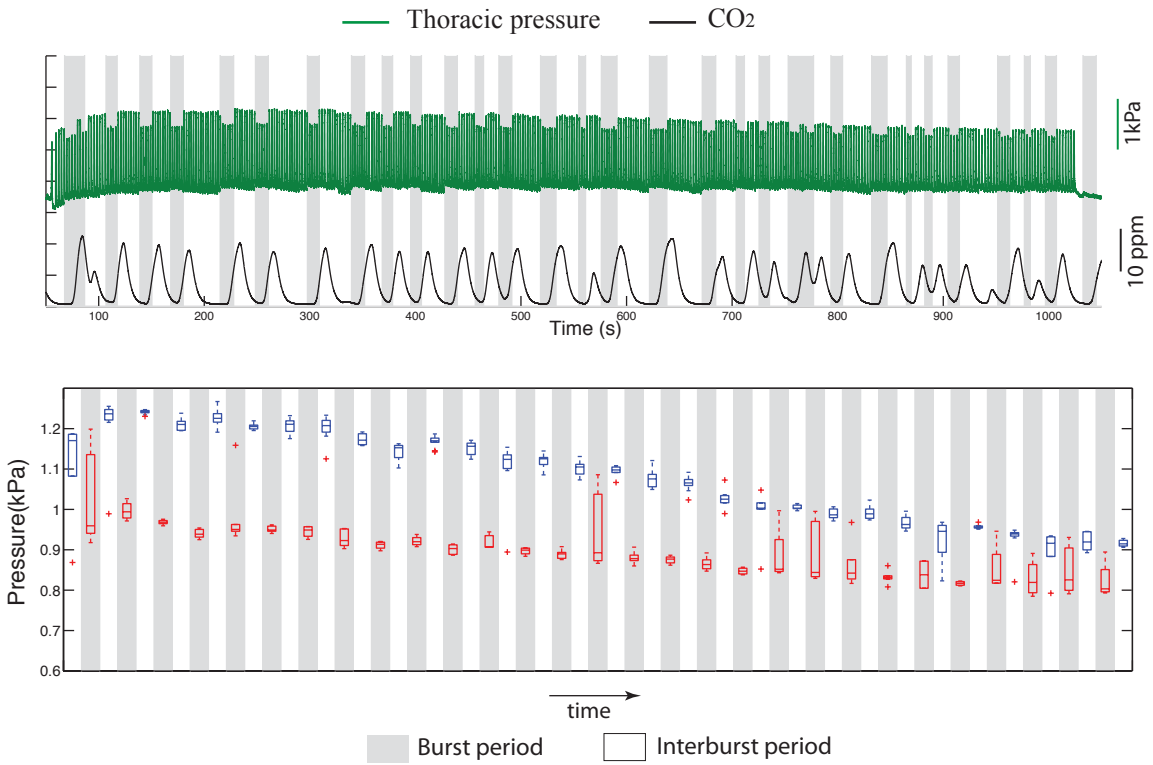

Pupa 8 - sequence 5

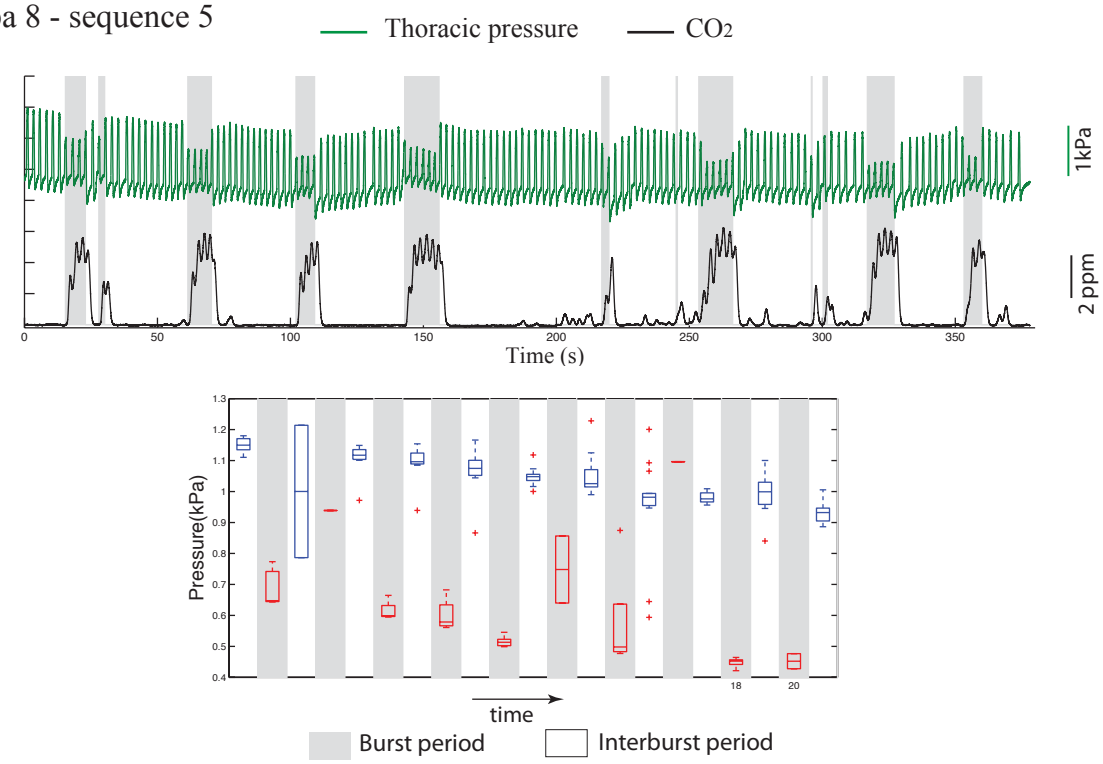

Pupa 9 - sequence 1

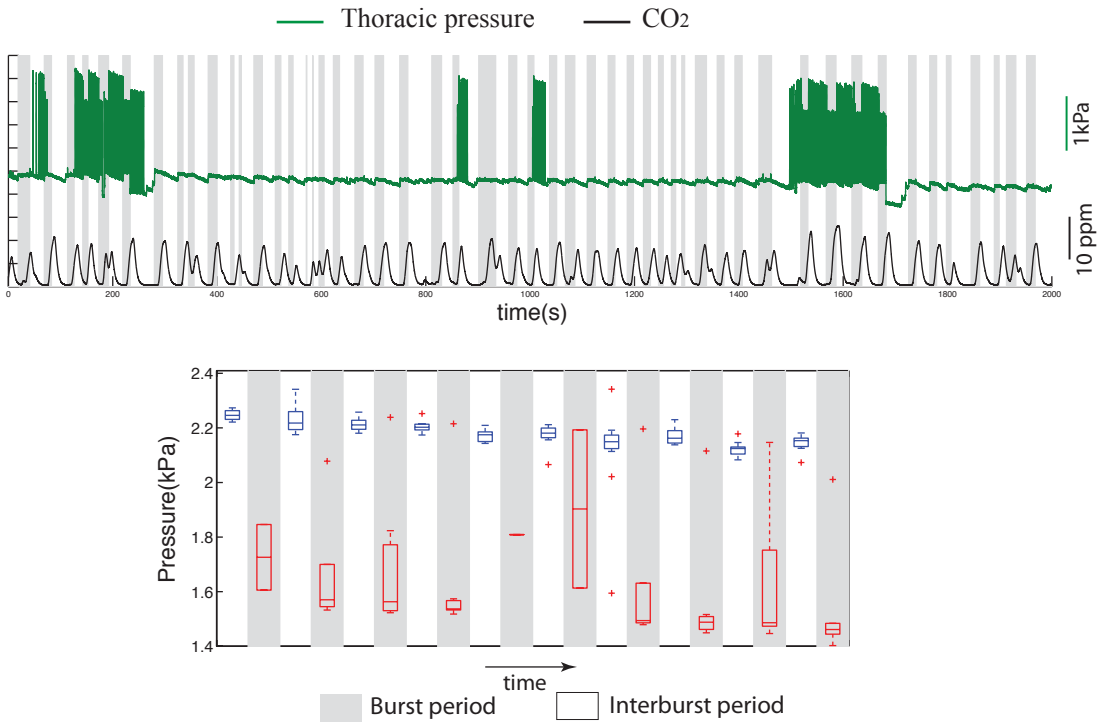

Pupa 9 - sequence 2

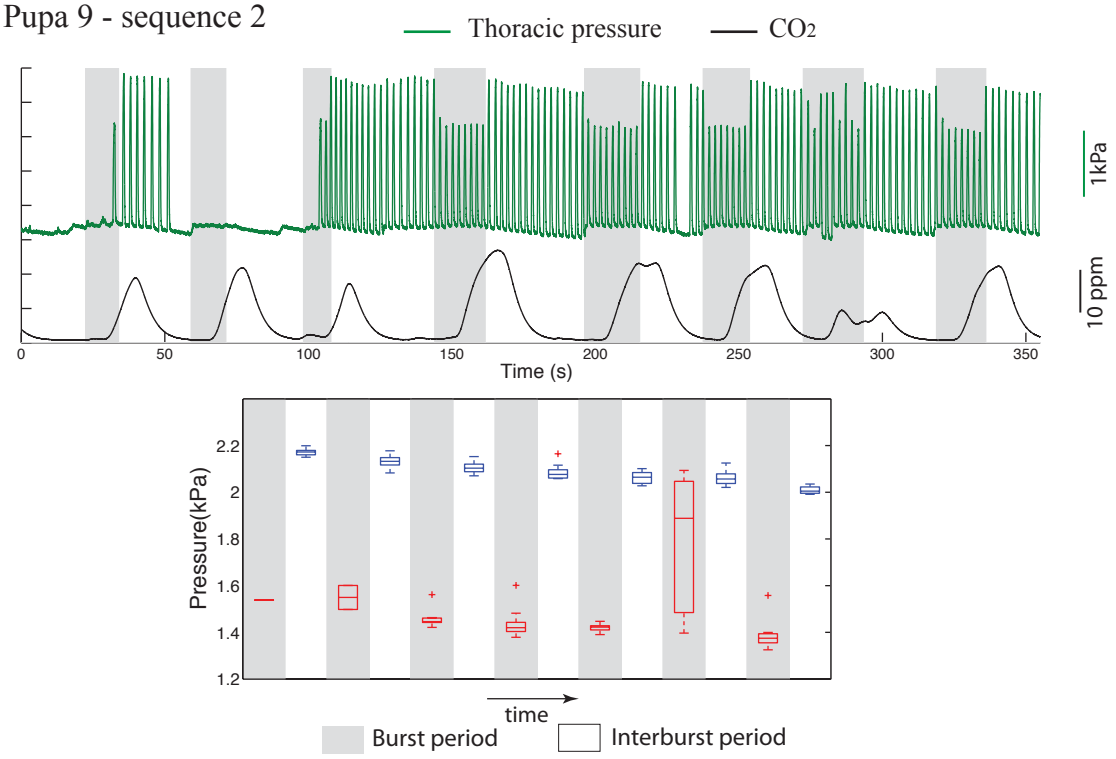

Pupa 9 - sequence 3

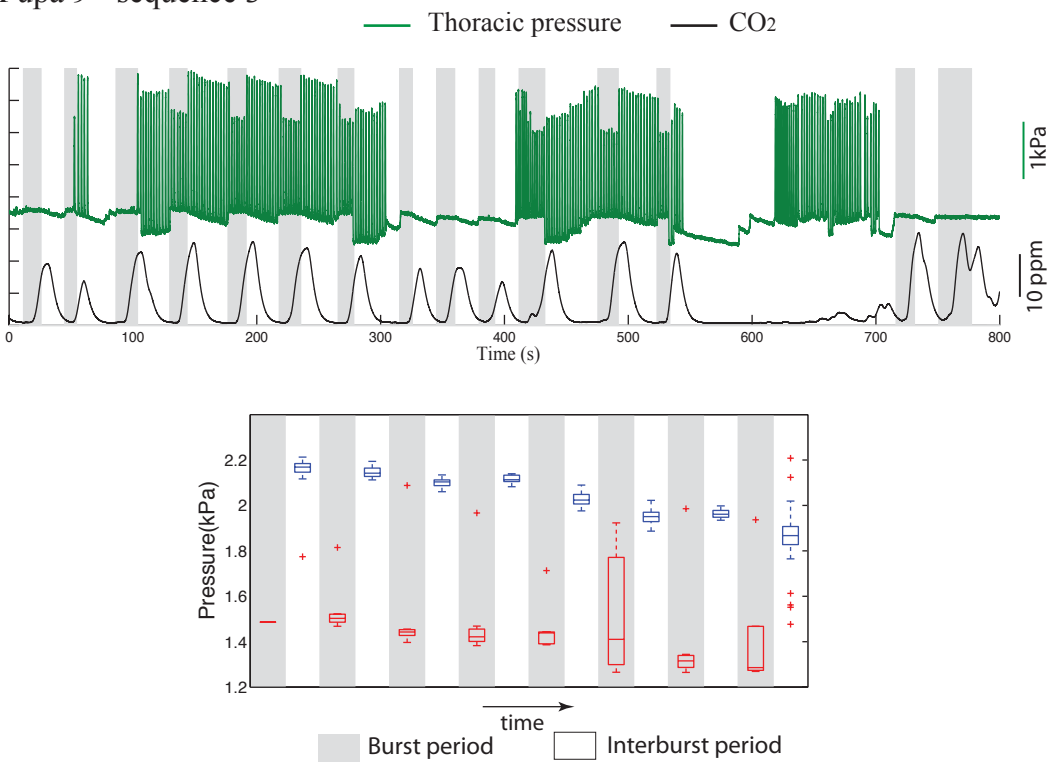

Pupa 9 - sequence 4

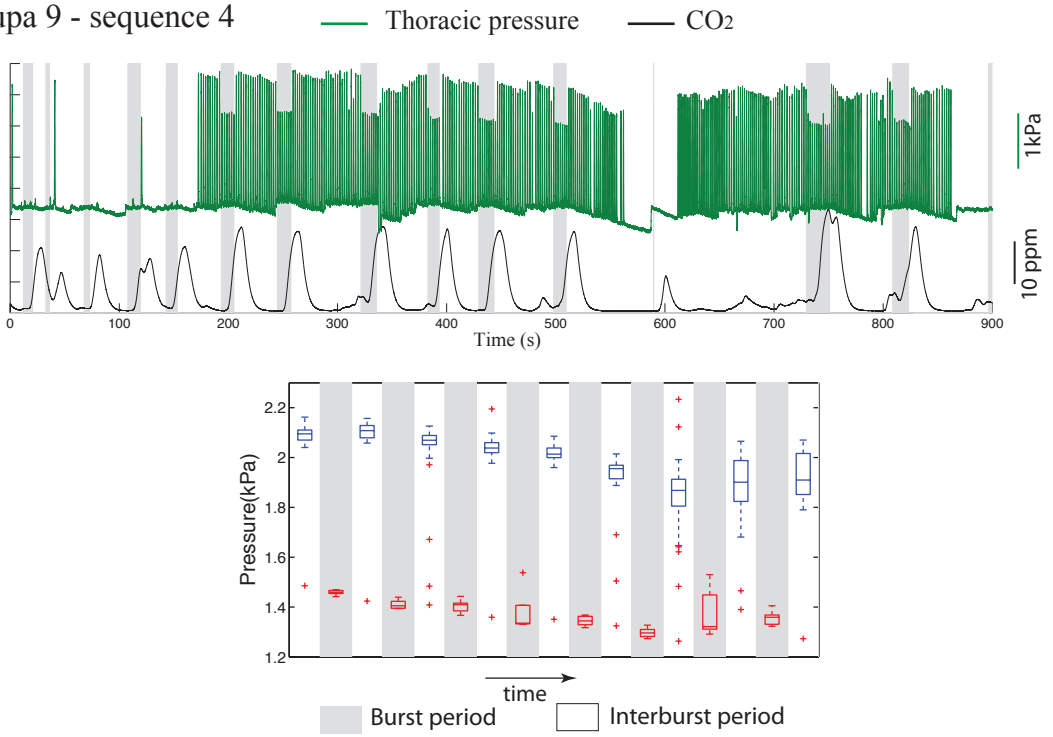

Pupa 10 - sequence 1

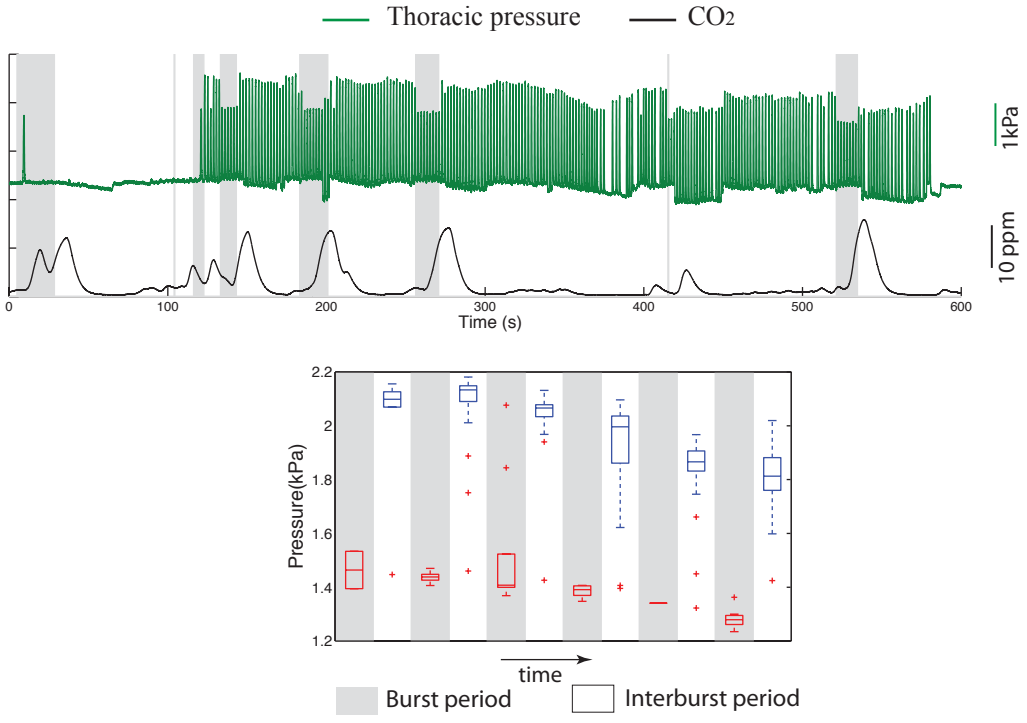

Pupa 11 - sequence 1

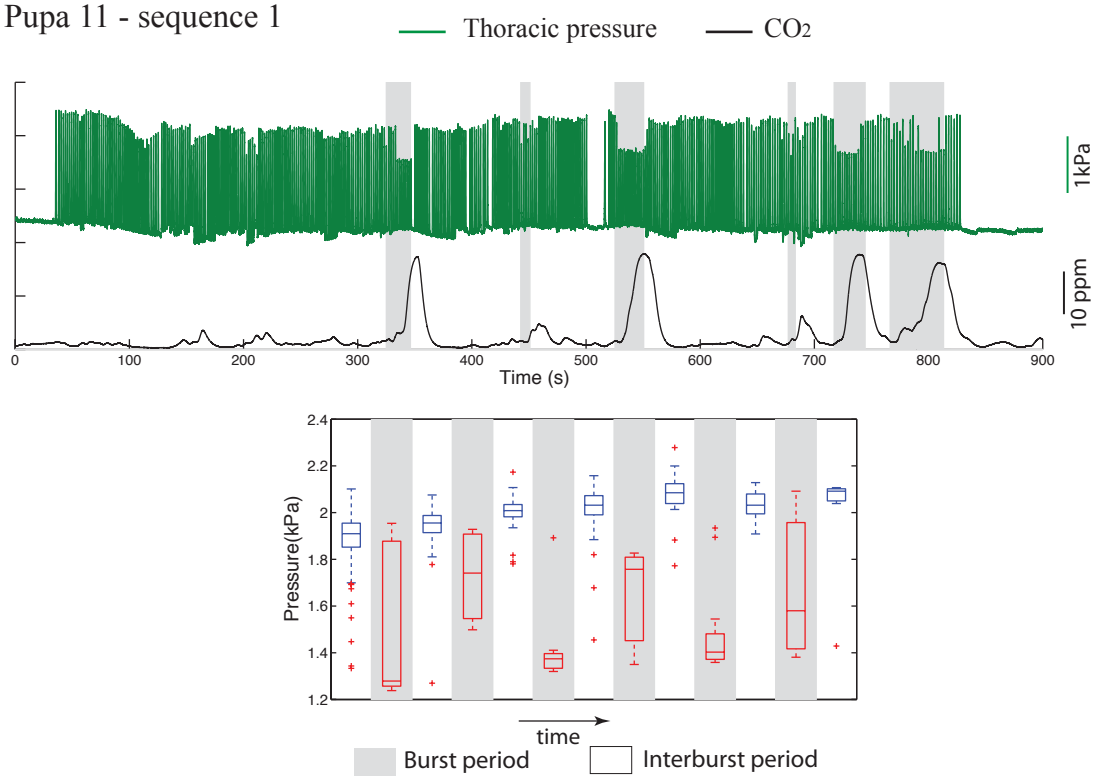

Pupa 11 - sequence 2

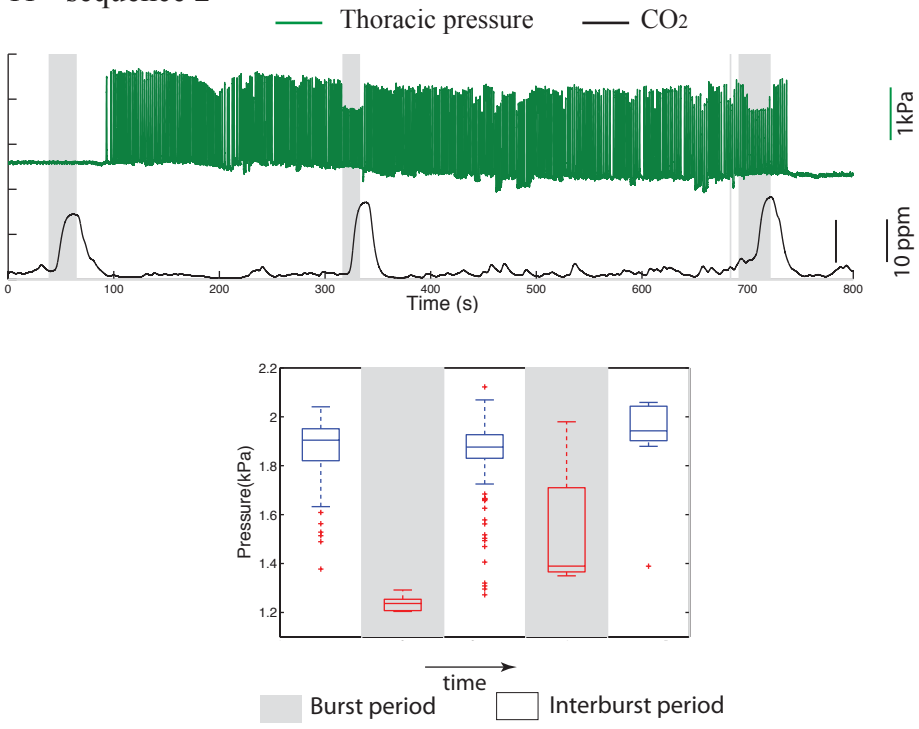

Pupa 12 - sequence 1

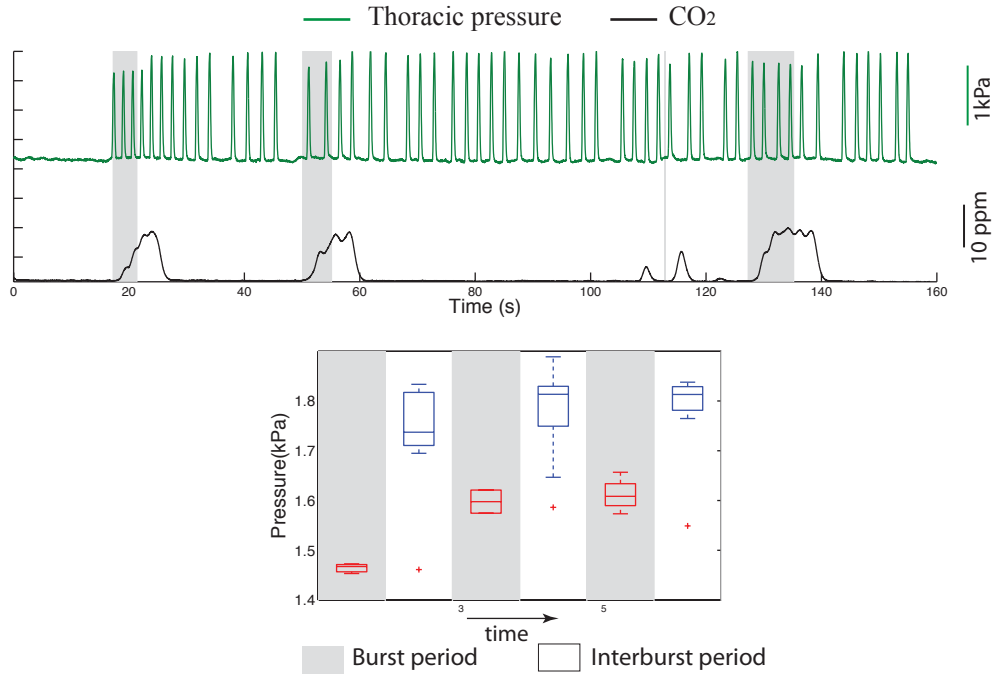

Pupa 13 - sequence 1

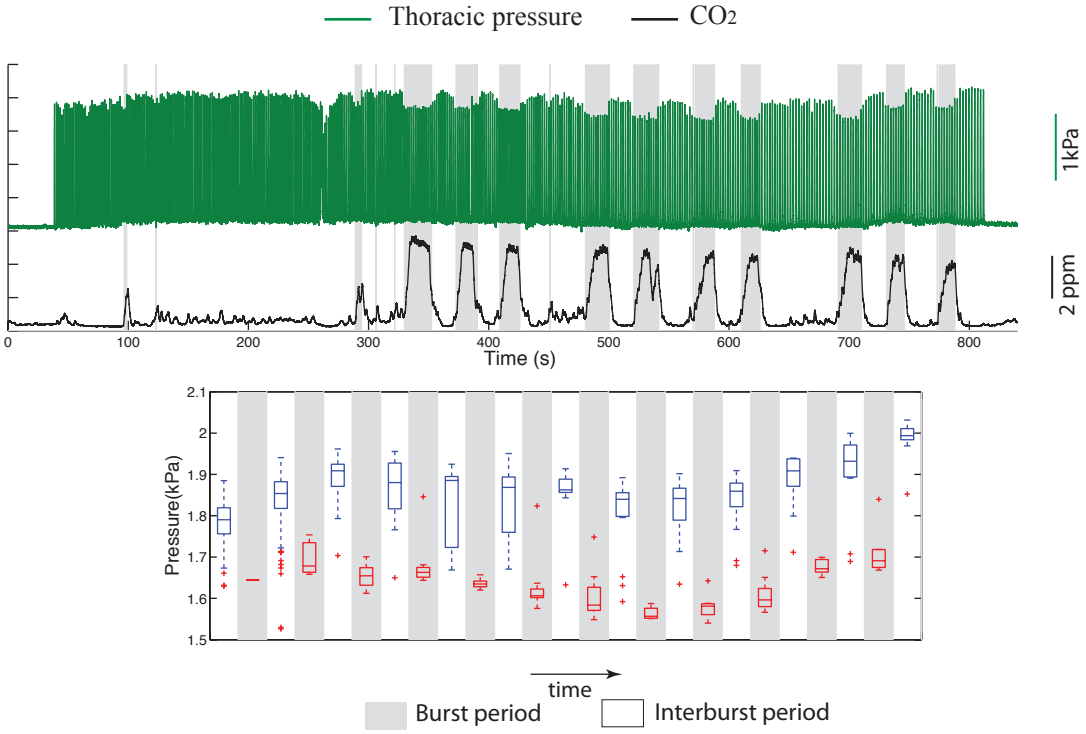

Pupa 13 - sequence 2

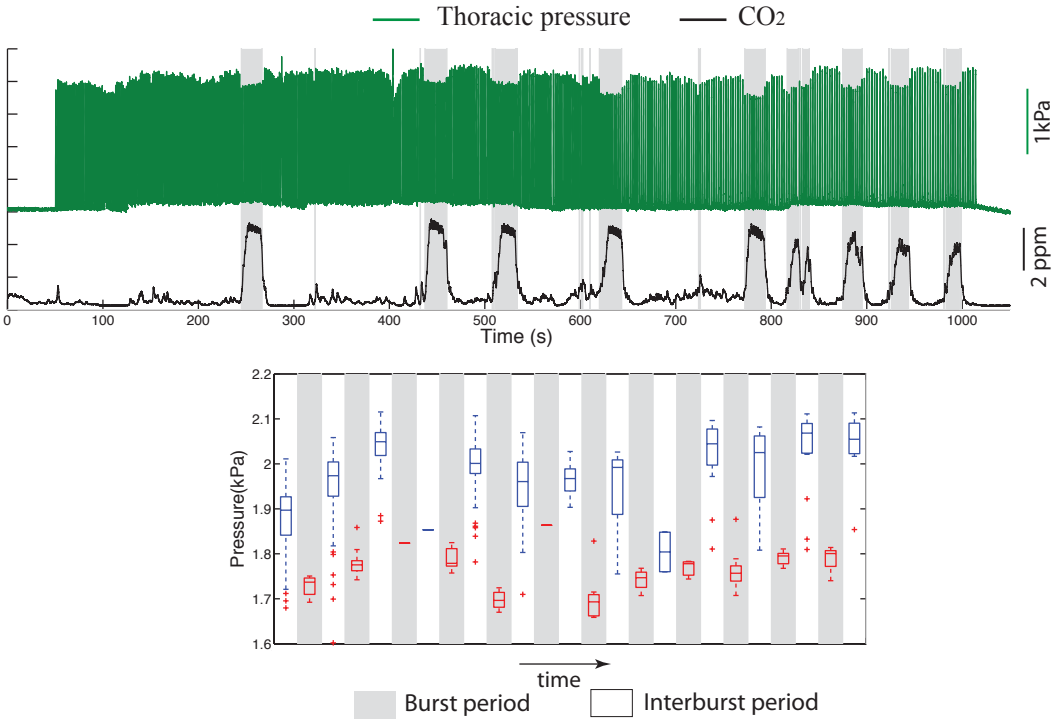

Pupa 14 - sequence 1